# Synthesis of Polyacetylene-like modified Graphene Oxide Aerogel and its Enhanced Electrical Properties

Enrico Greco†‡, Jing Shang*†, Jiali Zhu†, Tong Zhu*†

† State Key Joint Laboratory of Environmental Simulation and Pollution Control, College of Environmental Sciences and Engineering, and Center for Environment and Health, Peking University, 5 Yiheyuan Rd, Beijing, P.R. China, 100871.

‡ Beijing Innovation Center for Engineering Science and Advanced Technology (BIC-ESAT), Peking University, 5 Yiheyuan Rd, Beijing, P.R. China, 100871.

**ABSTRACT:** A graphene-based or carbon-based aerogel is a three-dimensional (3D) solid material in which the carbon atoms are arranged in a sheet-like nanostructure. In this study, we report the synthesis of low-density polymer-modified aerogel monoliths by 3D macro-assemblies of graphene oxide sheets that exhibit significant internal surface areas (982 $m^2/g$) and high electrical conductivity (~0.1 to 1 × $10^2$ S/cm). Different types of materials were prepared to obtain a single monolithic solid starting from a suspension of single-layer graphene oxide (GO) sheets, and a polymer, made from the precursors 4-carboxybenzaldehyde and polyvinyl alcohol. These materials were used to cross-link the individual sheets by covalent bonds, resulting in wet-gels that were supercritically dried and then, in some cases, thermally reduced to yield graphene aerogel composites. The average densities were approaching 15-20 $mg/cm^3$. This approach allowed for the modulation of distance between the sheets, pore dimension, surface area, and related properties. This specific GO/Polymer ratio has suitable malleability making it a viable candidate for use in conductivity 3D printing; it also has other properties suitable for energy storage, catalysis, sensing and biosensing applications, bioelectronics, and superconductors.

## 1. Introduction

Graphene and graphene oxide are a one-atom-thick planar two-dimensional (2D) sheets of carbon atoms, sp2-bonded, with a dense honeycomb-packed crystal lattice. The distinctive natural disposition of carbon atoms gives them a unique set of properties such as electronic, chemical, and mechanical. [1–4]

In the past few years, a significant number of researches have shown the potential applications of graphene-based sheets, and their impact in a wide range of technologies including energy storage,[5–9] catalysis,[10–13] sensing,[9,10,14] supercapacitors[15,16] and mechanically enhanced composites.[17–19] However, three-dimensional (3D) structures based on this extraordinary nanomaterial have not been well studied, and their synthesis or fabrication is limited to a few methods.[20,21,30,22–29]

*Corresponding author. E-mail: shangjing@pku.edu.cn (SHANG Jing)
*Corresponding author. E-mail: tzhu@pku.edu.cn (ZHU Tong)

Aerogels are 3D materials with open cell foam structures, high relative surface areas and nanoscale pores and cell sizes. One of the first developed and most commonly known aerogel is silica aerogel.[31–33] More recently it has been demonstrated that graphene can be used as building material for carbon-based aerogels composed of a network of different clustered carbon nanostructures.[34–36] Carbon-based aerogels show some similar properties to silica aerogels, but with different mechanical behaviors and a capacity for electrical conductivity that depends heavily on their density.[37–40] Some interactions with light have also been reported. Specifically, carbon-based aerogels can absorb light in the visible and infrared spectrums (they reflect only 0.3% of radiation between 250 nm and 14.3 μm).[41,42] The thermal conductivity of carbon aerogels tends to be equal to or less than air because these solids conduct heat only through thin chains of atoms, except for in the case of some specific structural modifications.[43–46] It would be desirable to develop three-dimensional composite nanostructures with the extraordinary functionalities of graphene and other materials that modulate aerogel properties.

Previous reports focused on the high stability of graphene oxide (GO) suspensions to assemble an initial GO macrostructure, which was then thermally reduced to yield a 3D graphene network[22,23]. While others used a polymer to reinforce the structure[47] because the GO aerogel (GOA) structure is usually maintained by non-covalent crosslink-like van der Waals forces without any chemo-electric bonds.[48] This resulted in a relative surface area lower than that of the 2D-GO,[49] and the bulk electrical conductivities of these assemblies only reached approximately $5 \times 10^{-1}$ S/cm[48,50] even in the case of metal doping.[50] This value is about five orders of magnitude lower than the conductivity reported for single graphene sheets.[50] Taken together, these results underscore the importance of generating or determining the physical bonds between the GO sheets while maintaining the original properties, which would increase the potential utility of 3D graphene macroassemblies.

In our study, we present a new method to obtain low-density graphene aerogels with high electrical conductivity, and large surface areas starting from GO, 4-carboxybenzaldehyde (4-CBA) and polyvinyl alcohol (PVA) to create an intrinsically conducting polymer (ICP) by dehydrogenation.[51,52] Also, to obtaining a conductive polymer during the first synthesis phase, another critical aspect in fabricating these macroassemblies was the formation of covalently bonded junctions between the ICP and individual graphene oxide sheets in order to reinforce the structure and provide electrical conductive interconnections between the sheets. The method presented here utilizes a precursor obtained by 4-CBA and PVA, the (Poly(4-formylperoxibenzoyl)acetylene to knit together graphene oxide sheets into a macroscopic 3D structure. With this approach, we are able to produce monolithic graphene oxide architectures with low densities (approaching 15-20 mg/cm$^3$) and electrical conductivities more than two orders

of magnitude higher than those reported for other graphene aerogels.[50] Furthermore, the relative surface areas are lower but comparable to the areas reported for 2D graphene sheets.[49,50]

## 2. Experimental

### 2.1 *Sample preparation*

The first two steps of our synthesis involved the preparation of the graphene oxide using the Hummers approach[53] to oxidize graphene flakes. The graphene oxide was then added to absolute ethanol (99.9%, Beijing Tongguang) to create a suspension. The solid content in the graphene oxide suspension may range from about 0.1 mg/mL to about 25 mg/mL as shown in Table 1. The suspensions were dispersed using a Shumei KQ-250DB ultrasonicator (frequency ~ 40 kHz, sonic power ~ 80 W). Six cycles of 15 minutes each of ultrasonication alternate with 15 minutes of stops were used to exfoliate the graphite oxide, and a sol-gel solution was finally obtained. It is crucial in this phase to reduce the time of each cycle and increase the number of cycles in order to avoid an increase of temperature of the solution and consequently a loss of functional groups on the surface of the single GO sheet. Any loss of oxygen on the GO surface could have negative effects on the formation of the covalent bonds with the polymer. Therefore this phase is extremely important and must be executed with maximum precision and attention.

The optimal conditions for GO dispersions were evaluated by a range of sonication cycles from 15 to 120 minutes.

**Table 1. List of samples**

| Sample name | GO susp. mg/ml | 4-CBA/PVA | Polymer/GO | Notes |
|---|---|---|---|---|
| GOA1 | 0.1 | 2:1 | 2:1 | The Polymer/GO ratio does not allow the formation of a proper structure. A wet-gel is formed, but the structure completely broke under SFE. |
| GOA2 | 0.5 | 2:1 | 1.5:1 | The result after the SFE process is not a monolith; the sample has not strong structural integrity. |
| GOA3 | 5 | 2:1 | 1:1 | |
| GOA4 | 10 | 2:1 | 1:1.5 | |
| GOA5 | 25 | 2:1 | 1:3 | |
| GOA6 | 25 | 2:1 | 1:10 | |
| GOA7 | 0.1 | 2:1 | 5:1 | The high Polymer/GO ratio does not allow the formation of a proper structure. The polymer tends to agglomerate. |

The ICP precursor was prepared in a solution of ethanol and Millipore water ranging from 0:1 to 99.9:1 v/v ratio using 4-carboxybenzaldehyde 98%, Alfa Aesar (it is possible to choose similar molecules with one carboxylic functional group), and a long chain polymer with at least two hydroxyl groups (such as polyvinyl alcohol 99+% hydrolyzed, Mw 146000-186000 Da, Sigma Aldrich). Hydroiodic acid (57 wt % in water) 0.1 wt% respect to PVA amount was used as a catalyst [51], under stirring for 2 hours. All the samples presented in this work was prepared using 99.9:0.1 v/v EtOH/H2O.

Electron Paramagnetic Resonance (EPR) spectrometry (EMXnano, Bruker, Germany) was applied for the detection of radicals during and after the reaction. The parameters for EPR measurements was set with a modulation frequency of 100 kHz, a microwave frequency of 9.61 GHz, a microwave power of 1.26 mW (19 dB), modulation amplitude of 2.0 G, a sweep width of 200 G, a time constant of 1.28 ms and 5 scans. A nitrone spin trapping agent (5,5-Dimethyl-1-pyrroline N-oxide ≥97%, DMPO, Sigma-Aldrich) was used to form stable spin adducts with radicals.

Fig. 1 shows the primary and the fitting EPR spectra of DMPO adducts. Spinfit results showed that in our reaction system two kinds of radicals including hydroxyl and peroxyl radicals formed, and the concentrations of hydroxyl and peroxyl radicals were $6.908\times10^{11}$ spins/mm$^3$ and $2.300\times10^{12}$ spins/mm$^3$, respectively. Control experiments showed that no radicals formed (Fig. 2-4), which confirmed that hydroxyl and peroxyl radicals were produced in our reaction system.

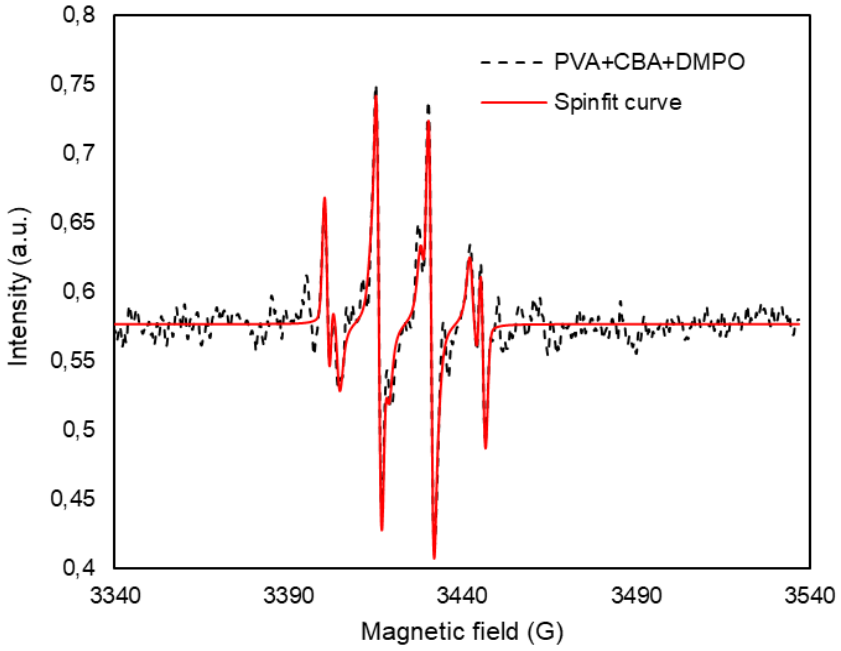


**Fig.1:** The primary and fitting EPR spectra of DMPO adducts.

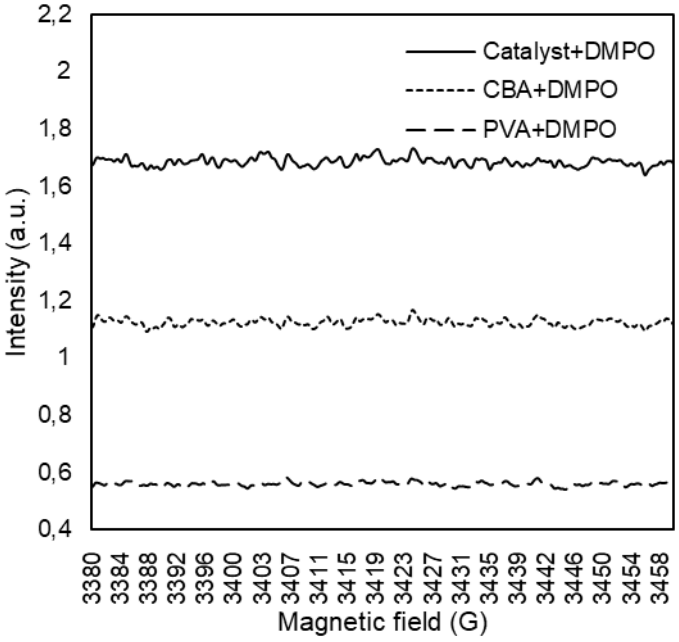


**Fig. 2:** The EPR spectra of three control experiments.

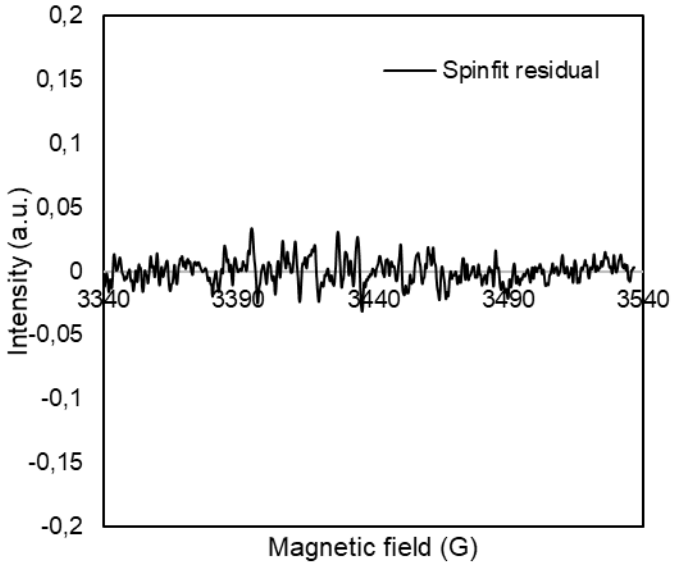


**Fig. 3:** The residual of spinfit curve.

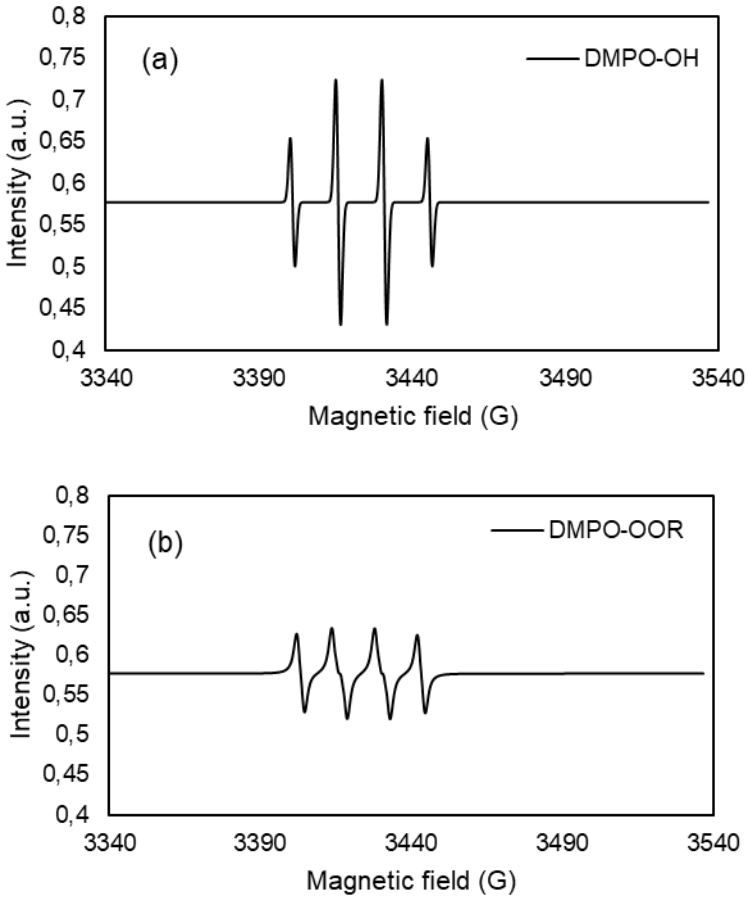


**Fig. 4:** The separate EPR spectra for DMPO-OH (a) and DMPO-OOR (b) adducts in the mixed fitting curve.

The formation of the wet-gel was first activated by the addition of the polymer solution to the GO solution and a mechanical shock, then was transferred to a Teflon Becker, sealed and cured in a water bath at 87°C for 5 hours. Sodium carbonate (anhydrous, 0.1 wt% respect to 4-CBA, Beijing Chemicals W.) was used as a catalyst. Polymer/GO wt ratio is typically in the range between about 0.1:1 to about 5:1. Depending on the application and the chemical/mechanical properties expected, other ratios could be suitable.

The resulted wet-gel was dried using an SFE-0.5 dryer using supercritical $CO_2$ at pressures of 7.5 to 8.0 ± 0.1 MPa and temperatures between 50.0 and 55.0 ± 0.5 °C. The system works with a flow rate of 1 $L \times h^{-1}$ using a separation chamber for the elimination of the extracted solvent and to obtain the samples shown in Figure 5. Some samples were pyrolyzed at 200°C under $N_2$ atmosphere for 6 hours in order to reduce all the graphene oxide to graphene. Any thermal treatment of the aerogel should be conducted under conditions that avoid the decomposition of the polymer network. A typical range should be about 120° to 450° C.


**Fig.5:** From the left: sample GOA4, GOA5, GOA6

## 3. Characterization

Field-Emission Scanning Electron Microscopy (FE-SEM) was performed on an FE-SEM LEO Supra 55 VP along with a GEMINI column (Carl Zeiss, Germany) 5-10 keV (20mA) in in-lens secondary electron imaging mode with a working distance of 2-8 mm, equipped with an Oxford Instrument Energy Dispersive Spectroscopy (EDX) analytical instrument.

FE-SEM showed a random and densely oriented 3D network sheet-like structures of the graphene aerogel (Figure 6a,b) similar to those seen in previous reports.[35,54] The sizes of the sheets ranged from hundreds of nanometers to several micrometers. Using a higher magnification, the GO sheets network was thin enough to be transparent (Figure 6a).

We did not observe any agglomeration or nanoparticles of polymer on the graphene oxide sheets or other sites, although more than half of the weight in the aerogel was attributed to the polymer. When the ICP: GO wt % ratio was more than 1:1, the polymerization and the formation of the GOA did not occur. It is also clear that a synthesis where the junctions are mediated by carbonyl and carboxyl functional groups instead of hydroxyl groups prevents the formation of polymer random-coils. In this case, the

physical crosslinks occur preferentially at the oxygen on the surface of the graphene oxide forming covalent bonds between individual sheets and the polymer formed a single macroassembly structure.

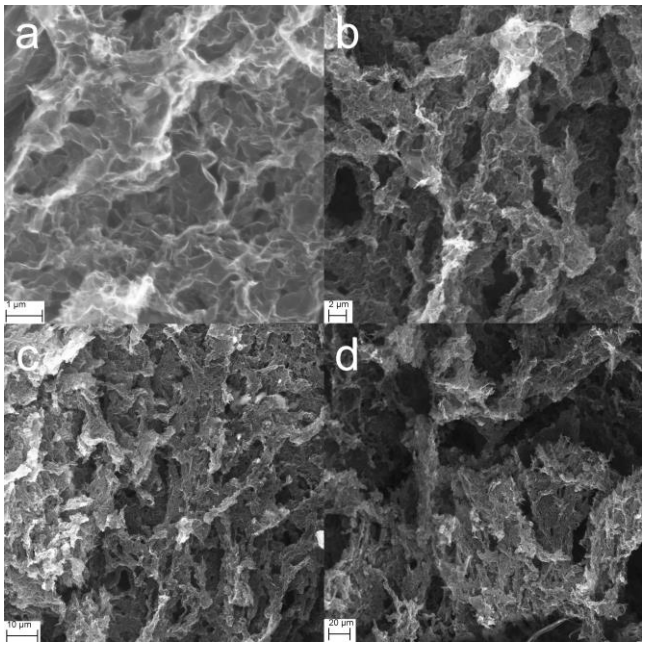


**Figure 6.** FE-SEM of the ICP-GO aerogel at different magnifications. It is possible to observe the porosity from a nanometer scale to micrometer.

Determination of the bulk densities was obtained from the physical dimensions and mass of each sample.

Relative Surface area and Pore Volume analysis were performed by Brunauer-Emmett-Teller (BET) and Barrett-Joyner-Halenda (BJH) methods by an ASAP 2000 Surface Area Analyzer (Micromeritics Instrument Corporation). Approximately 0.1 g of each sample was heated to 150°C under vacuum (10-5 Torr) overnight (at least 12 hours) to remove all adsorbed species. The list of results is reported in Table 1. The sample GOA1, GOA2, and GOA7 were not measured because of the reasons explained in the notes of Table 1.

The nitrogen adsorption/desorption isotherm for the ICP-GO-aerogel (Figure 7) showed a type IV curve, indicating that the material is mesoporous. The type three hysteresis loop[55,56] occurred at high relative pressure and was associated with adsorption in the nanoporous structures, consistent with the aggregates observed using FE-SEM. The pore size distribution for the aerogel was determined by the BJH method,[55] which showed no clear distribution of the pore volume with three different macrogroups: one lied in the 10-100 nm range, most in 100-1000 nm range and a little one in the 1000-10000 nm range (Table 2). The peak pore diameter was 126 nm. The BET surface area[57–59] for the aerogel strong-

ly depended on the ratio between polymer and GO during the synthesis, and the higher value was 982 $m^2/g$. The theoretical value of surface area for a single graphene oxide sheet is about 2600 $m^2/g$[50,60], but our samples showed lower values probably due to layering or overlapping of graphene oxide sheets within the assembly. Nevertheless, the measured surface area was higher than other values reported for high-quality GO-aerogels prepared via hydrogen arc discharge,[49] or GO-RF,[35,43] and it was three times higher than that of the CNT aerogel.[61]

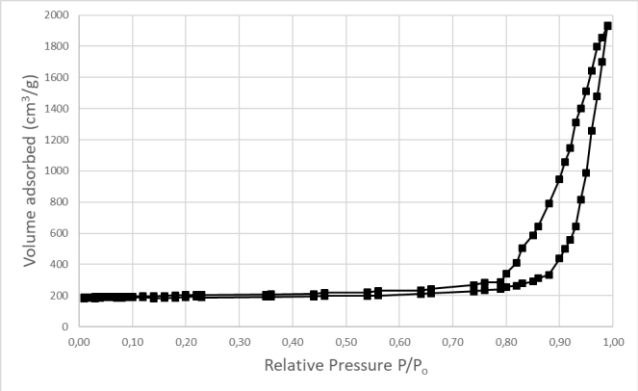


**Figure 7.** Nitrogen adsorption/desorption isotherm for the ICP-GO aerogel (GOA6)

The four-probe method was used to measure the electrical conductivity with metal electrodes attached to the ends of cylindrical samples. 100 mA of current was transmitted through the sample during the measurement, and the voltage drop was measured over distances of 6 to 7 mm. At least ten measurements were taken on each sample, and results were averaged and reported in Table 2.

**Table 2. Surface areas, pore volumes and electrical conductivity**

| Sample name | Relative surface areas (BET) $m^2/g$ | Pore volumes (BJH) 10-100 nm (%) | Pore volumes (BJH) 100-1000 nm (%) | Pore volumes (BJH) 1000-10000 nm (%) | Electrical conductivity S/cm |
|---|---|---|---|---|---|
| GOA1 | - | - | - | - | |
| GOA2 | - | - | - | - | |
| GOA3 | 557.4 | 44.1 | 32.4 | 23.5 | 12.3 |
| GOA4 | 719.3 | 51.0 | 37.3 | 11.7 | 31.6 |
| GOA5 | 788.7 | 48.2 | 31.6 | 20.2 | 54.2 |
| GOA6 | 982.2 | 62.8 | 25.2 | 12.0 | 128.1 |
| GOA7 | - | - | - | - | |

The bulk electrical conductivity (Table 2) of the polymer-modified graphene oxide aerogel was, (sample GOA6), 128 S/cm, about 2-3 orders of magnitude higher than those reported for other 3D graphene materials prepared with other methods.[48,50] It is our opinion that this extraordinarily high conductivity is due to a re-arrangement in the network morphology (many ripples in fixed positions) of the graphene oxide sheets in a 3D system. In congruence with the morphological differences, a substantial reduction in resistance at the connections between graphene sheets compared to those at the van der Waals bonds along with the use of an intrinsically conducting polymer could increase the mobility of the electrons and phonons. A more detailed discussion about the theoretical nature and the behavior of the charges in our polymer-modified aerogel will be presented in a forthcoming paper.

In conclusion, we prepared a macroscopic 3D polymer composite graphene oxide aerogel with large surface area and high electrical conductivity. Our approach used one molecule with a carboxyl and a carbonyl functional group to bind the hydroxyl group to a second molecule. It was used because of its long chain that could obtain conjugated bonds, and to space out the graphene oxide sheets. We were able to modulate the density, the pore dimension, and the conductivity just by changing the polymer:GO ratio. Due to these properties, these 3D graphene assemblies have potential relevance in a large number of applications as conductive 3D printing, energy storage, electrocatalysis, sensors and biosensors, and electro-biointerfaces.

## Acknowledgment

The authors are grateful to the financial support provided by National Natural Science Foundation of China (Grant Nos. 21876003, 21577003 and 41421064), the National Key Research and Development Program of China (No. 2016YFC0202200). The authors declare no competing financial interests. The authors want to acknowledge Dr. Joseph Valentine for the revision of the text.

## Author Contributions

EG conceived the methods, prepared the materials and made the characterizations, JZ made the EPR, JS, and TZ conceived the idea, coordinated the work and revised the manuscript.

## References

1 A. H. Castro Neto, F. Guinea, N. M. R. Peres, K. S. Novoselov and A. K. Geim, *Rev. Mod. Phys.*, 2009, **81**, 109–162.
2 K. A. Ritter and J. W. Lyding, *Nat. Mater.*, 2009, **8**, 235.
3 C. Mattevi, G. Eda, S. Agnoli, S. Miller, K. A. Mkhoyan, O. Celik, D. Mastrogiovanni, G. Granozzi, E. Garfunkel and M. Chhowalla, *Adv. Funct. Mater.*, 2009, **19**, 2577–2583.

M. A. Rafiee, J. Rafiee, Z. Wang, H. Song, Z.-Z. Yu and N. Koratkar, *ACS Nano*, 2009, **3**, 3884–3890.
R. Raccichini, A. Varzi, S. Passerini and B. Scrosati, *Nat. Mater.*, 2015, **14**, 271–279.
M. Pumera, *Energy Environ. Sci.*, 2011, **4**, 668–674.
J. Liu, J. S. Chen, X. Wei, X. W. Lou and X. W. Liu, *Adv. Mater.*, , DOI:10.1002/adma.201003759.
Z.-S. Wu, G. Zhou, L.-C. Yin, W. Ren, F. Li and H.-M. Cheng, *Nano Energy*, 2012, **1**, 107–131.
M. Pumera, *Chem. Rec.*, 2009, **9**, 211–223.
J. Shen, Y. Zhu, X. Yang and C. Li, *Chem. Commun.*, 2012, **48**, 3686.
B. F. Machado and P. Serp, *Catal. Sci. Technol.*, 2012, **2**, 54–75.
S. Sun, G. Zhang, N. Gauquelin, N. Chen, J. Zhou, S. Yang, W. Chen, X. Meng, D. Geng, M. N. Banis, R. Li, S. Ye, S. Knights, G. A. Botton, T.-K. Sham and X. Sun, *Sci. Rep.*, 2013, **3**, 1775.
X.-K. Kong, C.-L. Chen and Q.-W. Chen, *Chem. Soc. Rev.*, 2014, **43**, 2841–2857.

A. Di Mauro, R. Randazzo, S. F. Spanò, G. Compagnini, M. Gaeta, L. D'Urso, R. Paolesse, G. Pomarico, C. Di Natale, V. Villari, N. Micali, M. E. Fragalà, A. D'Urso and R. Purrello, *Chem. Commun.*, 2016, **52**, 13094–13096.
M. D. Stoller, S. Park, Y. Zhu, J. An and R. S. Ruoff, *Nano Lett.*, 2008, **8**, 3498–3502.
M. F. El-Kady and R. B. Kaner, *Nat. Commun.*, 2013, **4**, 1475.
M. Fang, K. Wang, H. Lu, Y. Yang and S. Nutt, *J. Mater. Chem.*, 2009, **19**, 7098–7105.
L. Baldino, M. Sarno, S. Cardea, S. Irusta, P. Ciambelli, J. Santamaria and E. Reverchon, *Ind. Eng. Chem. Res.*, 2015, **54**, 8147–8156.
P. Innocenzi, L. Malfatti and D. Carboni, *Nanoscale*, 2015, **7**, 12759–12772.
X. Mi, G. Huang, W. Xie, W. Wang, Y. Liu and J. Gao, *Carbon N. Y.*, 2012, **50**, 4856–4864.
F. Meng, X. Zhang, B. Xu, S. Yue, H. Guo and Y. Luo, *J. Mater. Chem.*, 2011, **21**, 18537–18539.
M. A. Worsley, P. J. Pauzauskie, T. Y. Olson, J. Biener, J. H. Satcher and T. F. Baumann, *J. Am. Chem. Soc.*, 2010, **132**, 14067–14069.
Y. Cheng, S. Zhou, P. Hu, G. Zhao, Y. Li, X. Zhang and W. Han, *Sci. Rep.*, 2017, **7**, 1–11.
W. Chen, S. Li, C. Chen and L. Yan, *Adv. Mater.*, 2011, **23**, 5679–5683.
Z. Tang, S. Shen, J. Zhuang and X. Wang, *Angew. Chemie*, 2010, **122**, 4707–4711.
J. L. Vickery, A. J. Patil and S. Mann, *Adv. Mater.*, 2009, **21**, 2180–2184.
F. Liu and T. S. Seo, *Adv. Funct. Mater.*, 2010, **20**, 1930–1936.
Y. Xu, K. Sheng, C. Li and G. Shi, *ACS Nano*, 2010, **4**, 4324–4330.
S.-Z. Zu and B.-H. Han, *J. Phys. Chem. C*, 2009, **113**, 13651–13657.
X. Zhang, Z. Sui, B. Xu, S. Yue, Y. Luo, W. Zhan and B. Liu, *J. Mater. Chem.*, 2011, **21**, 6494–6497.
A. Soleimani Dorcheh and M. H. Abbasi, *J. Mater. Process. Technol.*, 2008, **199**, 10–26.
D. W. Schaefer and K. D. Keefer, *Phys. Rev. Lett.*, 1986, **56**, 2199–2202.
J. L. Gurav, I.-K. Jung, H.-H. Park, E. S. Kang and D. Y. Nadargi, *J. Nanomater.*, 2010, **2010**, 1–11.
Z. Lin and X. Wang, *Angew. Chemie*, 2013, **125**, 1779–1782.
M. A. Worsley, S. O. Kucheyev, J. H. Satcher, A. V. Hamza and T. F. Baumann, *Appl. Phys. Lett.*, 2009, **94**, 073115.
B. S. Lalia, F. E. Ahmed, T. Shah, N. Hilal and R. Hashaikeh, *Desalination*, 2015, **360**, 8–12.
M. Sarno, L. Baldino, C. Scudieri, S. Cardea, P. Ciambelli and E. Reverchon, *J. Supercrit. Fluids*, 2016, **118**, 119–127.
X. Zhang, Z. Sui, B. Xu, S. Yue, Y. Luo, W. Zhan and B. Liu, *J. Mater. Chem.*, 2011, **21**, 6494.
H. Sun, Z. Xu and C. Gao, *Adv. Mater.*, 2013, **25**, 2554–2560.
C. Zhu, T. Y.-J. Han, E. B. Duoss, A. M. Golobic, J. D. Kuntz, C. M. Spadaccini and M. A. Worsley, *Nat. Commun.*, 2015, **6**, 6962.
US 8,871,821 B2, 2008.
N. Dabidian, I. Kholmanov, A. B. Khanikaev, K. Tatar, S. Trendafilov, S. H. Mousavi, C. Magnuson, R. S. Ruoff and G. Shvets, *ACS Photonics*, 2015, **2**, 216–227.
S. A. Al-Muhtaseb and J. A. Ritter, *Adv. Mater.*, 2003, **15**, 101–114.
L. W. Hrubesh and R. W. Pekala, *J. Mater. Res.*, 1994, **9**, 731–738.
X. Lu, R. Caps, J. Fricke, C. T. Alviso and R. W. Pekala, *J. Non. Cryst. Solids*, 1995, **188**, 226–234.
X. Lu, O. Nilsson, J. Fricke and R. W. Pekala, *J. Appl. Phys.*, 1993, **73**, 581–584.
H. Bai, C. Li, X. Wang and G. Shi, *Chem. Commun.*, 2010, **46**, 2376–2378.
F. Liu, C. Wang and Q. Tang, *Small*, 2018, **14**, 1–10.
Z. S. Wu, W. Ren, L. Gao, J. Zhao, Z. Chen, B. Liu, D. Tang, B. Yu, C. Jiang and H. M. Cheng, *ACS Nano*, 2009, **3**, 411–417.
S. Nardecchia, D. Carriazo, M. L. Ferrer, M. C. Gutiérrez and F. Del Monte, *Chem. Soc. Rev.*, 2013, **42**, 794–830.
A. Sreeram, S. Krishnan, S. J. DeLuca, A. Abidnejad, M. C. Turk, D. Roy, E. Honarvarfard and P. J. G. Goulet, *RSC Adv.*, 2015, **5**, 88425–

88435.
52 F. Menegazzo, T. Fantinel, M. Signoretto and F. Pinna, *Catal. Commun.*, 2007, **8**, 876–879.
53 W. S. Hummers and R. E. Offeman, *J. Am. Chem. Soc.*, 1958, **80**, 1339.
54 E. Yoo, J. Kim, E. Hosono, H. Zhou, T. Kudo and I. Honma, *Nano Lett.*, 2008, **8**, 2277–2282.
55 E. P. Barrett, L. G. Joyner and P. P. Halenda, *J. Am. Chem. Soc.*, 1951, **73**, 373–380.
56 S. Lowell, J. E. Shields, M. A. Thomas and M. Thommes, *Characterization of porous solids and powders: surface area, pore size and density*, 2004.
57 L. D. Gelb and K. E. Gubbins, *Langmuir*, 1998, **14**, 2097–2111.
58 G. Pickett, *J. Am. Chem. Soc.*, 1945, **67**, 1958–1962.
59 S. Brunauer, P. H. Emmett and E. Teller, *J. Am. Chem. Soc.*, 1938, **60**, 309–319.
60 A. Peigney, C. Laurent, E. Flahaut, R. R. Bacsa and A. Rousset, *Carbon N. Y.*, 2001, **39**, 507–514.
61 M. A. Worsley, P. J. Pauzauskie, S. O. Kucheyev, J. M. Zaug, A. V. Hamza, J. H. Satcher and T. F. Baumann, *Acta Mater.*, 2009, **57**, 5131–5136.